CityU Scholars

A high-entropy alloy as very low melting point solder for advanced electronic packaging

Liu, Y.; Pu, L.; Yang, Y.; He, Q.; Zhou, Z.; Tan, C.; Zhao, X.; Zhang, Q.; Tu, K.N.

Published in:
Materials Today Advances

Published: 01/09/2020

Document Version:
Final Published version, also known as Publisher's PDF, Publisher's Final version or Version of Record

License:
CC BY-NC-ND

Publication record in CityU Scholars:
Go to record

Published version (DOI):
10.1016/j.mtadv.2020.100101

Publication details:
Liu, Y., Pu, L., Yang, Y., He, Q., Zhou, Z., Tan, C., Zhao, X., Zhang, Q., & Tu, K. N. (2020). A high-entropy alloy as very low melting point solder for advanced electronic packaging. *Materials Today Advances*, *7*, [100101]. https://doi.org/10.1016/j.mtadv.2020.100101

Citing this paper
Please note that where the full-text provided on CityU Scholars is the Post-print version (also known as Accepted Author Manuscript, Peer-reviewed or Author Final version), it may differ from the Final Published version. When citing, ensure that you check and use the publisher's definitive version for pagination and other details.

General rights
Copyright for the publications made accessible via the CityU Scholars portal is retained by the author(s) and/or other copyright owners and it is a condition of accessing these publications that users recognise and abide by the legal requirements associated with these rights. Users may not further distribute the material or use it for any profit-making activity or commercial gain.

Publisher permission
Permission for previously published items are in accordance with publisher's copyright policies sourced from the SHERPA RoMEO database. Links to full text versions (either Published or Post-print) are only available if corresponding publishers allow open access.

Take down policy
Contact lbscholars@cityu.edu.hk if you believe that this document breaches copyright and provide us with details. We will remove access to the work immediately and investigate your claim.

Download date: 28/08/2022

Materials Today Advances 7 (2020) 100101

Contents lists available at ScienceDirect

Materials Today Advances

journal homepage: www.journals.elsevier.com/materials-today-advances/

A high-entropy alloy as very low melting point solder for advanced electronic packaging

Y. Liu [a,*], L. Pu [a], Y. Yang [b,c,**], Q. He [b], Z. Zhou [b], C. Tan [a], X. Zhao [a], Q. Zhang [a], K.N. Tu [d]

[a] Department of Materials Science and Engineering, Beijing Institute of Technology, Beijing, China
[b] Department of Mechanical Engineering, City University of Hong Kong, Hong Kong, China
[c] Department of Materials Science and Engineering, City University of Hong Kong, Hong Kong, China
[d] Department of Materials Science and Engineering, University of California, Los Angeles, USA

A R T I C L E I N F O

Article history:
Received 1 June 2020
Received in revised form
6 July 2020
Accepted 7 July 2020
Available online 14 August 2020

Keywords:
Pb-free solder
Diffusion kinetics
Liquid-solid reactions
High-entropy alloy
Advanced electronic packaging technology

A B S T R A C T

SnBiInZn-based high-entropy alloy (HEA) was studied as a low reflow temperature solder with melting point around 80 °C. The wetting angle is about 52° after reflow at 100 °C for 10 min. The intermetallic compound (IMC) growth kinetics was measured to be ripening-control with a low activation energy about 18.0 kJ/mol; however, the interfacial reaction rate is very slow, leading to the formation of a very thin IMC layer. The low melting point HEA solder has potential applications in advanced electronic packaging technology, especially for biomedical devices.
© 2020 The Author(s). Published by Elsevier Ltd. This is an open access article under the CC BY-NC-ND license (http://creativecommons.org/licenses/by-nc-nd/4.0/).

1. Introduction

While Moore's law in Si chip technology is approaching to its physical and economical limit, electronic packaging technology is becoming critically important to sustain the future computational growth in microelectronics industry. The trend in miniaturization of very-large-scale-integration is moving from 2D IC to 3D integrated circuit (IC) [1–3]. The latter has various chips stacking vertically, which requires the development of new technologies such as through-Si-Via and microbumps. More importantly, the 3D IC packaging technology will need to use a hierarchy of solder joints. In other words, low (around 100 °C), middle (200 °C), and high (300 °C) wetting temperature solders will work together, so that different components can be stacked and integrated. At the moment, we have the high-Pb $Pb_{95}Sn_5$ solder for the high melting point and the eutectic SnAg solder for the middle melting point [4,5]. But for the low melting point, we only have eutectic SnBi, which has a melting point of 138 °C with a soldering temperature about 150 °C [6,7]. It would be better if we could lower the soldering temperature furthermore to 100 °C. Moreover, as the increase of electronics diversity, we are seeing the development of soft electronics, biomedical devices, solar cells, and so on. For these applications, it is important to have low reflow temperature solder applied to related packaging technologies because the working temperature of these devices is low.

How to develop industrial applicable Sn-based low melting point solders will be problematic. Eutectic binary Sn-based solders have been studied for decades; however, so far we have no appropriate solders with a melting point below 180 °C, not to say solders with a melting point below 100 °C that can be applied to biomedical devices. Because binary Sn-based solder can no longer fit itself to the fast technology development, the research on multicomponent solder is essential. Multicomponent alloys have the unique properties in the form of high-entropy alloy (HEA), especially in creep resistance [8], magnetic properties [9], biocompatibility [10], deformation behavior [11], and sluggish diffusion effect [12]. The application of HEA alloys as solders may bring these unique properties to solders, which can bring up a new area in the design of solders and broaden the applications of solders. In this article, we explore an HEA alloy as solder. The solder

* Corresponding author.
** Corresponding author.
E-mail addresses: yingxia.liu@bit.edu.cn (Y. Liu), yonyang@cityu.edu.hk (Y. Yang).

https://doi.org/10.1016/j.mtadv.2020.100101
2590-0498/© 2020 The Author(s). Published by Elsevier Ltd. This is an open access article under the CC BY-NC-ND license (http://creativecommons.org/licenses/by-nc-nd/4.0/).

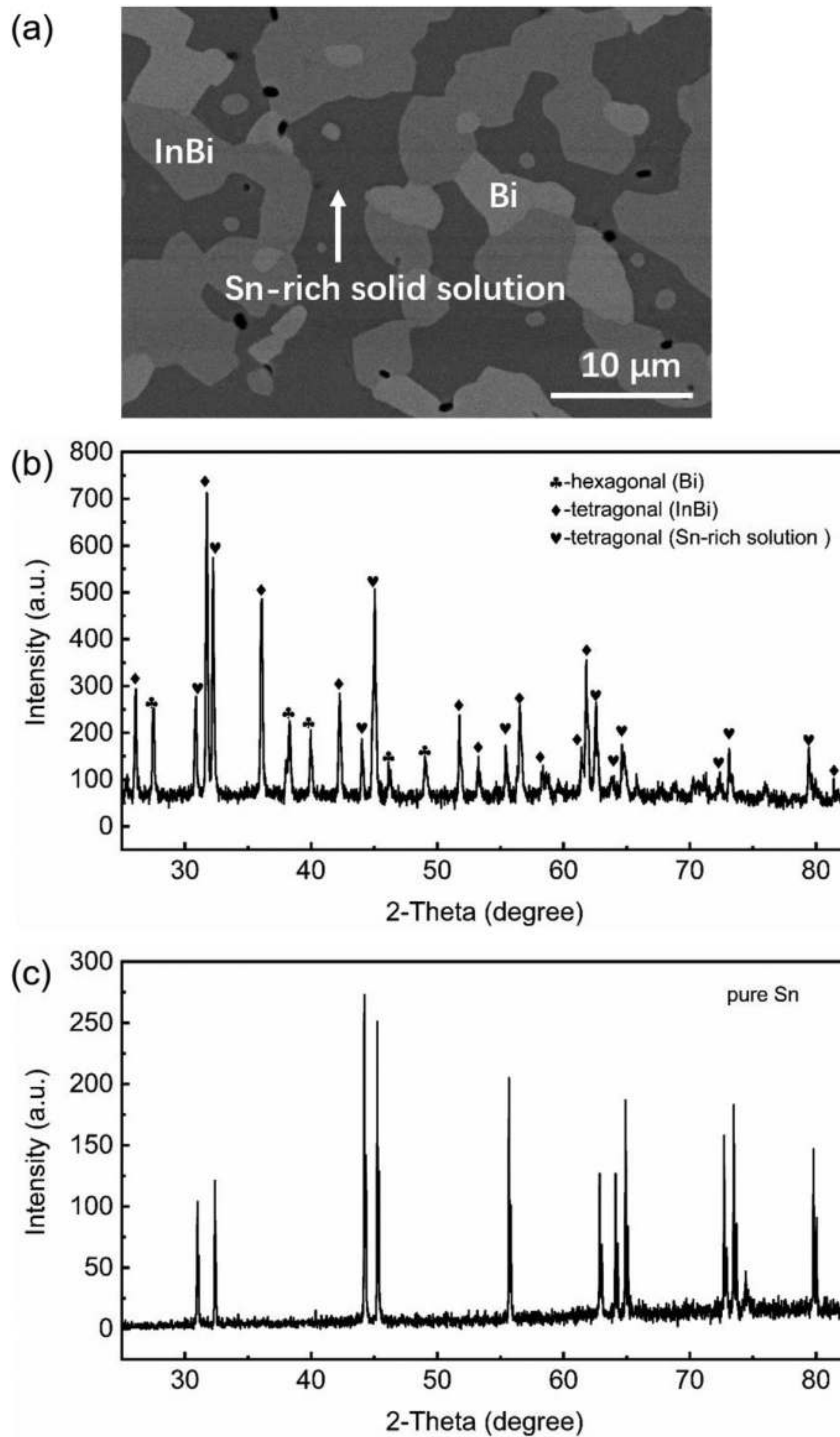

Fig. 1. (a) The SEM image of the original HEA solder. (b) and (c) XRD results of the HEA solder and pure Sn. HEA, high-entropy alloy; SEM, scanning electron microscope; XRD, X-ray diffraction.

has a melting point as low as 80 °C and a solder wetting temperature about 100 °C.

2. Experimental

SnBiInZn HEA solder were prepared using high purity (>99.9%) Sn, Bi, In and Zn as atomic ratio of Sn:Bi:In:Zn = 1:1:1:1 in a vacuum induction furnace. Pieces about 5–10 mg were cut from the bulk solder alloy. These pieces were analyzed by differential thermal analysis (DTA) to measure the melting point of SnBiInZn solder.

To study the wetting behavior, we polished copper foils with 2.5 μm diamond abrasion paste and cleaned with deionized water. Then a piece of 0.5 mg solder was placed on the copper foil merging in flux and reflowed on a hot-plate at 120 °C, 140 °C and 160 °C for

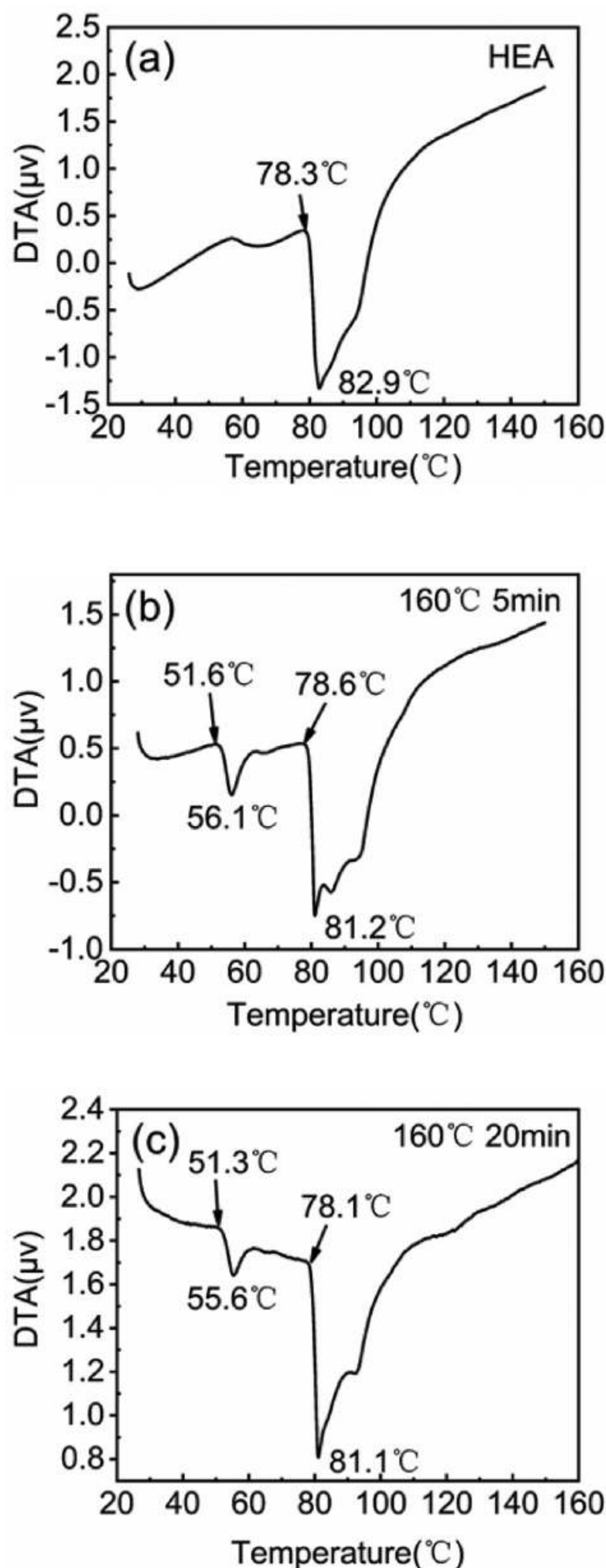

Fig. 2. (a) DTA result for original HEA material; (b) and (c) DTA result for HEA after being reflowed at 160 °C for 5 min and 20 min. HEA, high-entropy alloy; DTA, differential thermal analysis.

5 min, 10 min, and 20 min, respectively. We also succeeded to wet the HEA solder on a Cu plate at 100 °C for 10 min and 20 min. After reflow, we cooled the samples in air to room temperature and cleaned the samples with pure alcohol.

The wetting samples were mounted in epoxy resin. The cross-sections were polished with SiC papers successively and then with 0.04 μm SiO_2 powder suspension. We observed the cross-sections of the polished samples by scanning electron microscope (SEM). The elemental composition of interfacial intermetallic compound (IMC) was analyzed by using energy-dispersive X-ray spectroscope (EDX). We measured the area and length of IMC by Image J. The thickness of IMC was obtained from area divided by length. Transmission electron microscope (TEM) images were acquired by FEI Themis Z FEG/TEM operated at 200 kV in bright-field (BF) scanning tunneling electron microscopy (STEM) mode and by high-angle annular dark-field (HAADF) STEM mode for more detailed information. High-resolution TEM (HRTEM) images are also acquired. The TEM-ready samples were prepared using the in situ focused ion beam (FIB) lift out technique on a FEI G4 HX dual beam FIB/SEM. The samples were capped with e-carbon and I-carbon before milling. The TEM lamella thickness was ~60 nm.

For shear tests, we reflowed 5 ± 0.5 mg of diced solder pieces on 1 mm diameter circular Cu substrate at 120 °C–160 °C for 1 min, 5 min, and 20 min. We collected four sets of data for each testing condition. The shear tests were performed using PTR-1100 shear test machine at room temperature with a shear strain rate of 0.5 mm/s.

3. Results and discussions

3.1. Interfacial microstructure and HEA solder matrix

SEM cross-sectional image of original HEA solder is shown in Fig. 1(a). There are three phases observed in Fig. 1(a): the Sn-rich phase, InBi phase, and Bi phase. Fig. 1(b) and (c) are the X-ray diffraction (XRD) results of the original HEA solder and pure Sn, respectively. By comparison, we can see the Sn-rich phase in the alloy has broader peaks than pure Sn; in addition, there is a tiny shift in the peak position, implying the Sn-rich phase is a solid solution. It needs to be noted that, we do have InBi and Bi phase in the alloy and the entropy of this alloy may not be as high as other HEAs. But the Sn-rich phase in the alloy does have a solid solution structure, and for that phase, it has a high entropy. The HEA solder structure seems to be very stable, and there is no big difference before and after reflow. More characterization results about the Sn-rich solid solution phase after reflow reaction will be presented.

DTA was performed to find the solder melting point around 80 °C, as shown in Fig. 2(a). After being reflowed at 160 °C for 5 min and 20 min, another small peak around 56 °C occurred in the DTA curve, shown in Fig. 2(b) and (c), indicating that some phase transformation had taken place inside the HEA material during the reflow. Fig. 3(a)–(d) show the wetting angle after soldering for 10 min at 100 °C–160 °C. The wetting angle is about 35–40° after soldering at 120 °C–160 °C for different length of time but more than 50° at 100 °C. When we further reduced the reflow time to 1 min, we noticed that at the reflow temperature of 140 °C and 160 °C, we can have successful soldering. However, we were unable to achieve repetitively good solder joint at the reflow temperature of 100 °C and 120 °C with just 1 min reflow time. Often, we obtained a very thin layer of IMC (less than 200 nm) in the solder joints after reflow. We tend to believe that the flux is not quite efficient at such a low working temperature (100 °C and 120 °C). Our future work would include the finding of a flux with a low working temperature at 100 °C for 1 min reflow.

The microstructure of the HEA cap, as well as the interfacial structure between the HEA and Cu was observed by SEM cross-sectional images and FIB. Fig. 4(a) and (b) are, respectively, the lower (1000X) and the higher (6000X) magnification cross-sectional SEM images of the solder after reflowing at 100 °C for

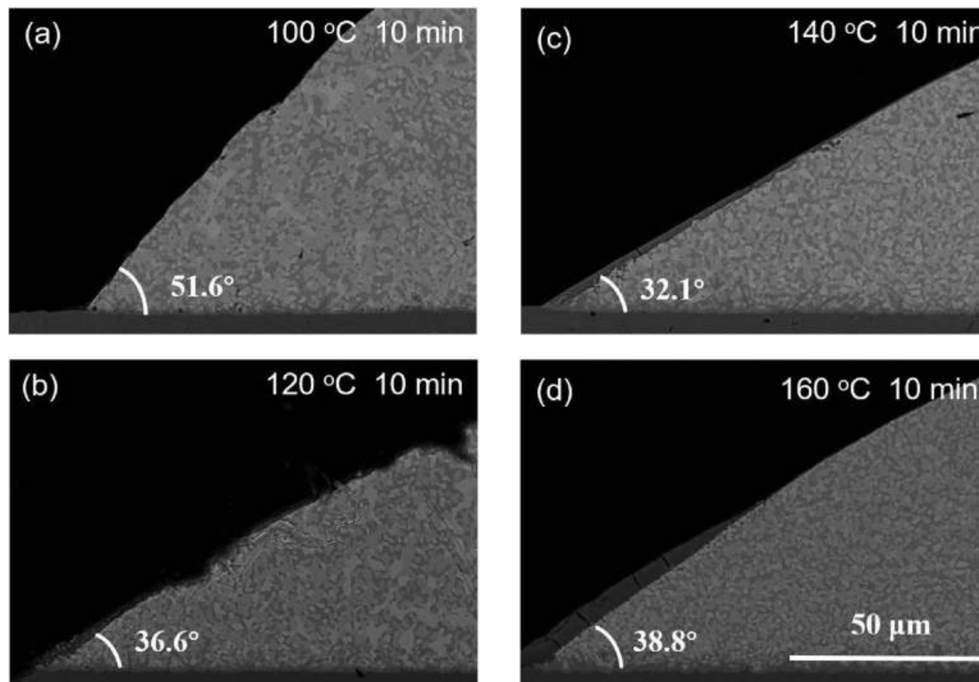

Fig. 3. (a)–(d) The wetting angles after being reflowed for 10 min at different temperatures, (a) 100 °C; (b) 120 °C; (c) 140 °C; (d) 160 °C.

20 min, and the uniform HEA solder microstructure can be observed. Fig. 4(c) shows the cross-sectional FIB ion beam image of the solder after reflowing for 5 min at 160 °C. Fig. 4(d) shows the SEM cross-sectional image for the solder after reflowing for 20 min at 160 °C. In accordance with the EDX results, shown in Fig. 4(e), the IMC formed during soldering reaction is believed to be Cu_6Sn_5 with a few percent of In substituting Sn atoms. The microstructure of the HEA cap is very complicated and has at least three detectable phases, including the phases of almost pure Bi phase, InBi phase, and Sn-rich phase, as marked in both Fig. 4(b) and (d). These three phases have also been confirmed by XRD. In the ion beam image in Fig. 4(c), more information could be revealed, where three to four different phases with different extent of gray could be seen. Some twin structure is observed in one of those phases, which is marked by the white arrow. In the IMC part, there seems to be two layers of IMCs, marked by the two black arrows.

To have a better understanding of the HEA solder matrix and the formed IMC after reaction, TEM images in Fig. 5 were obtained after the solder being reflowed for 5 min at 160 °C. Fig. 5(a) is a BF STEM image, and we can observe solder layer, IMC layer, and Cu layer in the image. Fig. 5(b) is a higher magnification BF TEM image, and two layers of IMC can be distinguished. Fig. 5(c) is a HAADF STEM image, and we can observe some Kirkendall voids located between IMC and the Cu substrate. In the IMC layer, there are some tiny darker spots. From the EDX results, shown in Fig. 5(d), where we did EDX line scan along the arrow in Fig. 5(a), we tend to regard those two layers as Cu_3Sn and Cu_6Sn_5 with a few percent of Zn and In. The results consist with the EDX results obtained from SEM. Fig. 5(e)–(h) are to show the element Cu, In, Sn, and Zn element distribution and the EDX mapping area is indicated in the white rectangular in Fig. 5(a). As shown in Fig. 5(h), Zn element appears to be particles in the EDX mapping image, thus, those tiny spots in IMC might be Zn particles.

Fig. 6(a) is the same as Fig. 5(a) used to mark the detected locations. The diffraction pattern of the solder layer with zone axis of [1 0 1] is shown in Fig. 6(b). The solder matrix has body-centered tetragonal (bct) structure with measured lattice parameters a = b = 0.676 nm, c = 0.339 nm. Compared with Sn bct crystal structure, a = b = 0.583 nm, c = 0.318 nm, the measured lattice constants are about 10% distorted from pure Sn. The reason should be explained by the 30 at. % In and a few percent of Zn atoms in the lattice. The atomic radius of Sn, In, and Zn is 145 pm, 155 pm, and 135 pm, respectively [13]. We also obtained HRTEM images to show the lattice sites, as shown in Fig. 6(c), (d) and (e). Those images are acquired in locations marked in the red rectangular shown in Fig. 6(a). The three locations are around a hole, induced during the thinning when we make the FIB-TEM sample. The three locations all have the same crystal structure as pure Sn. In accordance with Fig. 6, the solder matrix seems to have relatively large grains and each grain is a single crystal. We note that the solder composes of around 40 at. % In and Zn atoms; however, it still has perfect bct crystal structure. That is why we believe our solder is in high-entropy state. Though the solder may not be defined exactly as HEA because it has less than five main elements in it, it should be appropriate to define the solder as medium-entropy alloy. The application of HEA as solder in this work is a novel try and should have plenty of following work in the future.

3.2. Growth kinetics of IMCs

To study IMC growth kinetics, the thickness of the IMC formed at 120 °C, 140 °C, and 160 °C after different reflow time was measured. The relationship between mean thicknesses L and reaction time t, can be described very well by Eq. (1), and the growth rate D can be calculated using the following equation [6].

$$L = Dt^n \tag{1}$$

The Arrhenius relationship can be applied to obtain the activation energy, in the form given in the following context [6],

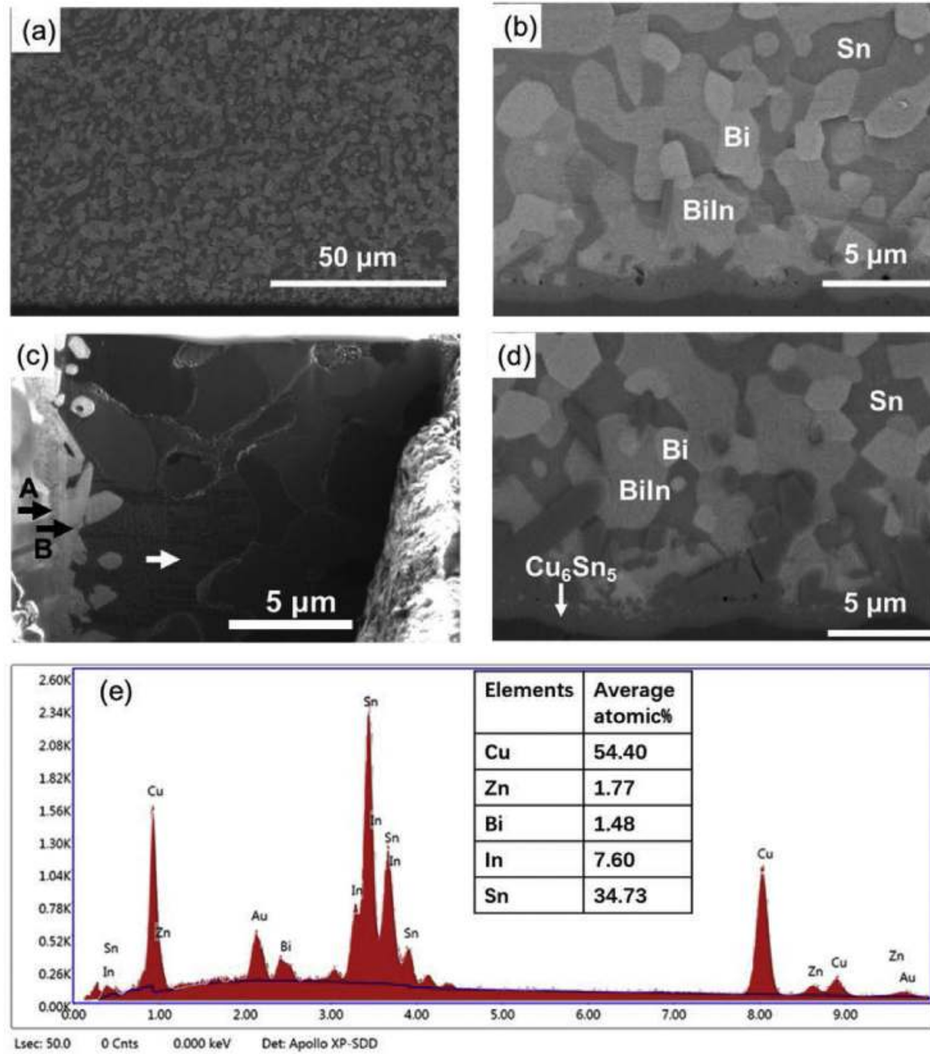

Fig. 4. (a) and (b). The lower (1000 X) and higher (6000 X) magnification SEM images of the solder after reflowing at 100 °C for 20 min; (c). The focused ion beam (FIB) ion beam image of the solder after reflowing for 5 min at 160 °C; (d). The SEM image for the solder after reflowing for 20 min at 160 °C; (e) the EDX result in the IMC area. IMC, interfacial intermetallic compound; SEM, scanning electron microscope; EDX, energy-dispersive X-ray spectroscope.

$$D = A\exp\left(-\frac{E_a}{RT}\right) \tag{2}$$

where n is a reaction constant and A is a prefactor, E_a is the activation energy, R is the ideal gas constant, and T is the absolute temperature. We fit the measured thickness and reaction time into the logarithm of Eq. (1) and obtain the calculated n to be 0.30 ± 0.04, 0.32 ± 0.13, and 0.36 ± 0.04 for 120, 140, and 160 °C, respectively, as shown in Fig. 7(a). Alternative to Eq. (1), ways of approximation can be tried. Considering the low accuracy of time exponent determination, we may assume n to be 1/3. This type of dependence is well known for the growth kinetics of Cu_6Sn_5 phase in interactions of Cu with tin-based liquid solder, where the published Cu_6Sn_5 has ripening growth kinetics with $n = 1/3$ [14,15]. The measured IMC thickness data is plotted to $t^{1/3}$ in Fig. 7(b). The activation energy is then calculated from the slopes of the fitted lines to be 18.0 kJ/mol, as shown in Fig. 7(c). Some published data on the activation energy for solid-liquid interfacial reactions of Cu-Sn has been reported to be 19.72 kJ/mol [16] and 29 kJ/mol, respectively [17]. The activation energy for Sn58Bi solder reaction with Cu is reported to be 17.6 kJ/mol [6] and eutectic SnPb solder reaction with Cu is 18.3–27.9 kJ/mol [13]. By comparison, we can figure that the activation energy we measured in HEA solder/Cu reaction is in the same range.

Significantly, while the activation energy of solid-liquid interfacial reaction of the HEA solder on Cu is in the same range as other conventional solders, the rate of IMC formation is much slower. It is worth noting that after HEA solder reflowing for 10 and 20 min at 100 °C, the average IMC thickness is measured to be 1.32 and 1.49 μm, respectively. This is surprising, and it could be a unique nature of the HEA alloy because the entropy factor is in the prefactor ‘A’ as shown in Eq. (2). In the temperature range of 100–160 °C, the solid-solid interfacial reaction occurs in the conventional solders. On the other hand, if we conduct solid-liquid interfacial reaction for 10–20 min, say in SnAg solder on Cu, the IMC will be over 10 μm [18], which is much thicker than that observed here. In theory, the prefactor $A \propto \exp\left(\frac{\Delta S}{R}\right)$ and S represents the activation entropy. Neglecting the change in vibrational entropy during the IMC formation, we may approximately take $\Delta S \approx S_{tran} - S_{HEA}$, where S_{tran} and S_{HEA}

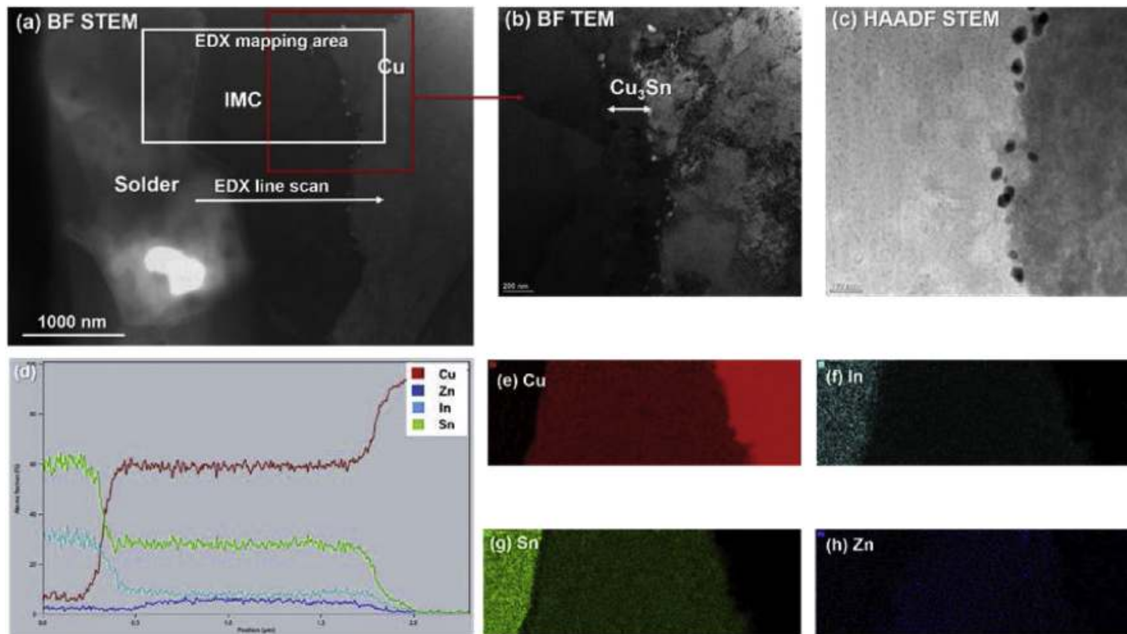

Fig. 5. TEM images after solder reflowing on Cu substrate at 160 °C for 5 min; (a) BF STEM image for the interface; (b) Higher magnification BF TEM image; (c) HAADF STEM image; (d) EDX line scan results; (e), (f), (g) and (h) EDX mapping to show the distribution of element Cu, In, Sn, and Zn. EDX, energy-dispersive X-ray spectroscope; TEM, transmission electron microscope; BF, bright field; STEM, scanning tunneling electron microscopy; HAADF, high-angle annular dark-field.

stand for the configurational entropy of the transition state and the original HEA, respectively, during IMC formation. Because S_{HEA} of HEAs is very high at a high homologous temperature, which could reach the prediction of the ideal mixing rule [19,20], we herein propose that the low prefactor A may be attributed to the entropy reduction during the IMC formation in the HEA. In case that $S_{tran} \ll S_{HEA}$, $A \propto \exp\left(-\frac{S_{HEA}}{R}\right)$ and hence, high configurational entropy could lead to rather low reaction kinetics, as seen in our experiments.

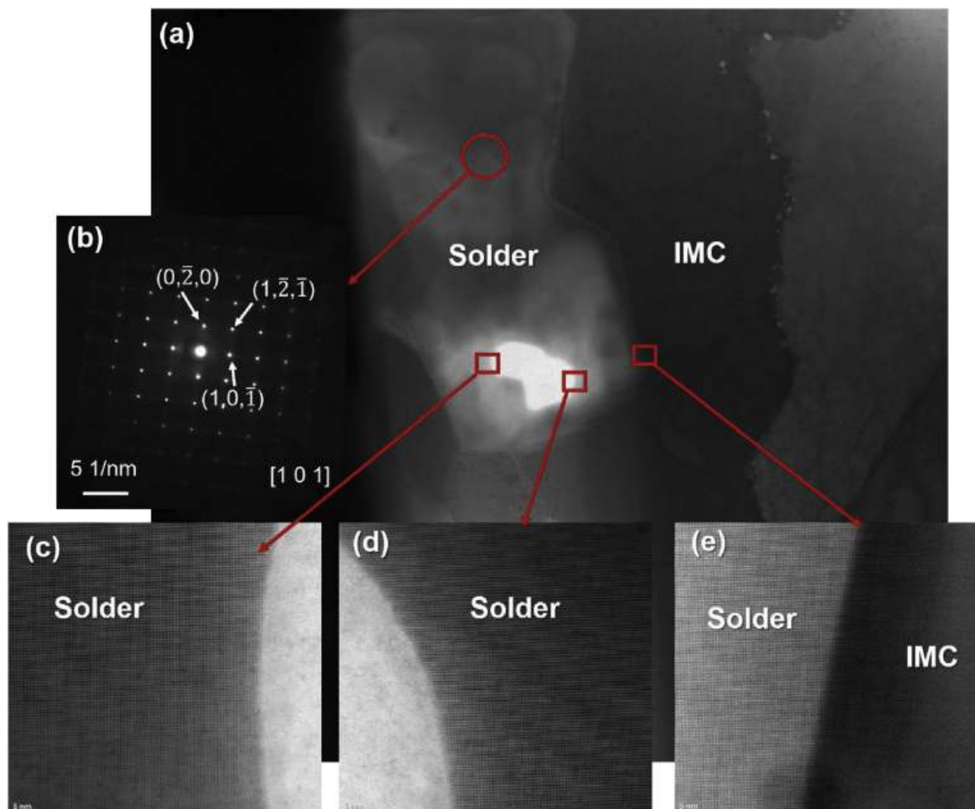

Fig. 6. (a) BF STEM image for the interface; (b) The diffraction pattern for solder area; (c), (d) and (e) HRTEM images to show solder matrix lattice sites. BF, bright field; STEM, scanning tunneling electron microscopy; HRTEM, high-resolution transmission electron microscope.

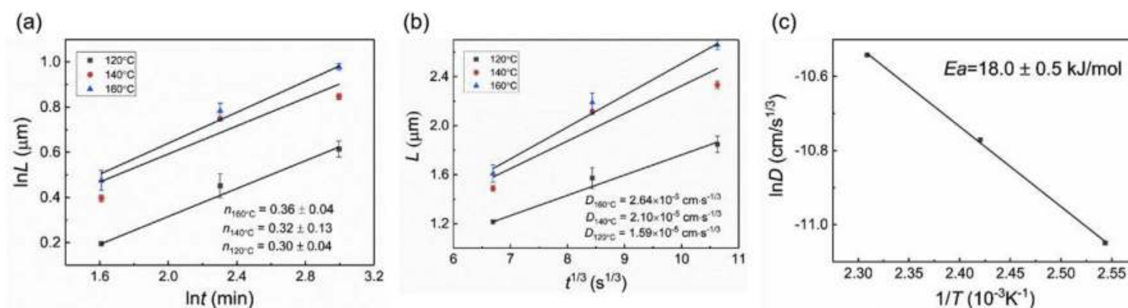

Fig. 7. (a) The logarithm fitting plot of L to t; (b) Measured IMC thickness plotted with $t^{1/3}$; and (c) Arrhenius-type plot of the growth rate constant to 1/T. IMC, interfacial intermetallic compound.

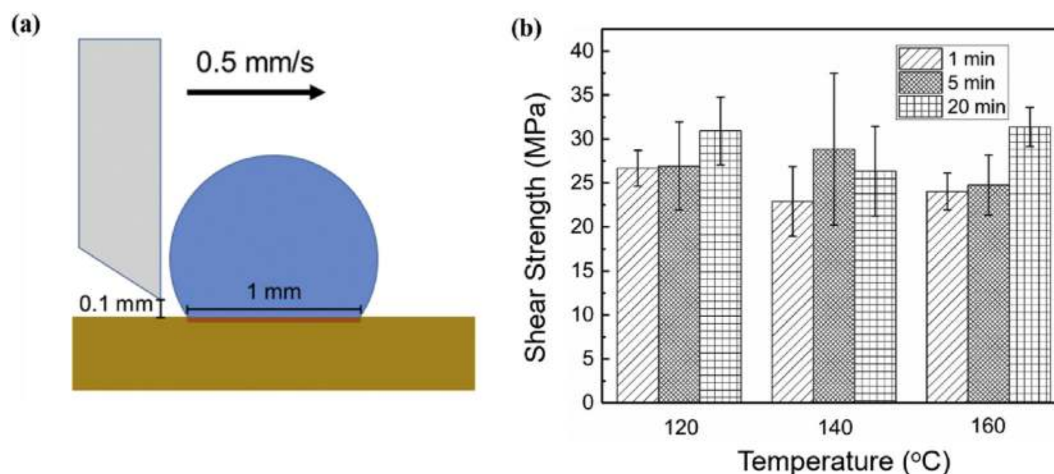

Fig. 8. (a) The schematic diagram to show shear test of solder joint; and (b) The shear strength of SnBiInZn solder joint.

It should be noted that, even after 20 min reflow at 100 °C, the IMC thickness is still very thin with an average thickness of 1.49 μm. If we could find a high efficiency flux and obtain a successful wetting solder joint at 100 °C, we expect a very thin layer of IMC in the joint after reflow for 1 min. The thin thickness of IMC layer could relieve many yield and reliability issues in the future small size solder joints. For example, we might not need the Ni layer as the diffusion barrier on the Cu under bump metallization to prevent the high Cu consumption rate, as well as Kirkendall void formation. The latter has been associated to the growth of a thick layer of Cu_3Sn between Cu_6Sn_5 and Cu [21–23]. This is because the void nucleation requires the supersaturation of vacancies in Cu_3Sn and in its interface with Cu. As shown in Fig. 5, there are only some tiny Kirkendall voids in our sample even after reflow for 5 min at 160 °C. Kirkendall voids–related reliability issues would be mitigated by our solder.

3.3. Shear test results

The mechanical properties of this low melting point solder joint were investigated by shear test and the test results are shown in Fig. 8. As shown in Fig. 8(b), we collected 4 sets of data for each testing condition and the average shear strength is measured to be about 22 MPa–31 MPa. In accordance with the published data, solders with different composition, including Sn-0.4Cu, Sn-3Ag-0.4Cu, Sn-58Bi, and SnZnBi, have the shear strength of 19.5 MPa, 32.5 MPa, 64 MPa, and 18.5–28.0 MPa, respectively [24–26]. Comparing with the published data, we conclude that the HEA solder joint has a relatively good mechanical strength. Especially, even though at 120 °C, we can only have a very thin layer of IMC, the solder joint strength is still good.

4. Conclusion

In summary, the HEA of SnBiInZn has been studied as a low melting point solder. It has good wetting properties and good shear strength at the reflow temperature of 100 °C. Moreover, the IMC growth kinetics study indicates that it has a very slow solid-liquid interfacial reaction rate during reflow, forming a very thin layer of Cu_6Sn_5 IMC. The reason was explained by the unique nature of the HEA alloy because the prefactor '*A*' in the Arrhenius relationship has the entropy factor. The application of HEA as low melting point solder in this work is a novel try, and it has potential for applications in advanced electronic packaging technology in the future.

Credit author statement

Yingxia Liu: Conceptualization, Methodology, Investigation, Writing Original Draft; **Li Pu**: Validation, Investigation; **Yong Yang**: Conceptualization. Writing - Review & Editing; **Quanfeng He**: Resources; **Ziqing Zhou**: Resources; **Chengwen Tan**: Project administration; **Xiuchen Zhao**: Project administration; **Qingshan Zhang**: Project administration; **K. N. Tu**: Supervision, Writing - Review & Editing

Data availability

The raw/processed data required to reproduce these findings cannot be shared at this time as the data also forms part of an ongoing study.

Declaration of competing interest

The authors declare that they have no known competing financial interests or personal relationships that could have appeared to influence the work reported in this paper.

Acknowledgements

The authors at Beijing Institute of Technology would like to acknowledge the financial support from Youth Program of National Natural Science Foundation of China with the project number 51901022. The research of YY is supported by City University of Hong Kong with the project number 9610391.

References

[1] Y. Liu, M. Li, D.W. Kim, S. Gu, K. Tu, Synergistic effect of electromigration and Joule heating on system level weak-link failure in 2.5 D integrated circuits, J. Appl. Phys. 118 (2015) 135304.
[2] K. Tu, Y. Liu, M. Li, Effect of Joule heating and current crowding on electromigration in mobile technology, Appl. Phys. Rev. 4 (2017), 011101.
[3] Y. Liu, Y.C. Chu, K. Tu, Scaling effect of interfacial reaction on intermetallic compound formation in Sn/Cu pillar down to 1 μm diameter, Acta Mater. 117 (2016) 146–152.
[4] A. Kroupa, D. Andersson, N. Hoo, J. Pearce, A. Watson, A. Dinsdale, S. Mucklejohn, Current problems and possible solutions in high-temperature lead-free soldering, J. Mater. Eng. Perform. 21 (2012) 629–637.
[5] R. Khazaka, L. Mendizabal, D. Henry, R. Hanna, Survey of high-temperature reliability of power electronics packaging components, IEEE T. Power Electron. 30 (2014) 2456–2464.
[6] J. Li, S. Mannan, M. Clode, D. Whalley, D. Hutt, Interfacial reactions between molten Sn–Bi–X solders and Cu substrates for liquid solder interconnects, Acta Mater. 54 (2006) 2907–2922.
[7] J. Li, S. Mannan, M. Clode, K. Chen, D. Whalley, C. Liu, D. Hutt, Comparison of interfacial reactions of Ni and Ni–P in extended contact with liquid Sn–Bi-based solders, Acta Mater. 55 (2007) 737–752.
[8] Y.L. Chou, Y.C. Wang, J.W. Yeh, H.C. Shih, The effect of molybdenum on the corrosion behavior of the high-entropy alloys Co1.5CrFeNi1.5Ti0.5Mox in aqueous environments, Corrosion Sci. 52 (2010) 1026–1034.
[9] C. Chen, H. Zhang, Y.Z. Fan, W.W. Zhang, R. Wei, T. Wang, T. Zhang, F.S. Li, A novel ultrafine-grained high entropy alloy with excellent combination of mechanical and soft magnetic properties, J. Magn. Magn Mater. 502 (2020) 5.
[10] W.-Y. Ching, S. San, J. Brechtl, R. Sakidja, M. Zhang, P.K. Liaw, Fundamental electronic structure and multiatomic bonding in 13 biocompatible high-entropy alloys, Comput. Mater. 6 (1) (2020) 45, npj.
[11] Y. Zhang, T.T. Zuo, Z. Tang, M.C. Gao, K.A. Dahmen, P.K. Liaw, Z.P. Lu, Microstructures and properties of high-entropy alloys, Prog. Mater. Sci. 61 (2014) 1–93.
[12] J.W. Yeh, Recent progress in high entropy alloys, Ann. Chim. Sci. Mat. 31 (6) (2006) 633–648.
[13] J.C. Slater, Atomic radii in crystals, J. Chem. Phys. 41 (1964) 3199–3204.
[14] H. Kim, K. Tu, Kinetic analysis of the soldering reaction between eutectic SnPb alloy and Cu accompanied by ripening, Phys. Rev. B Condens. Matter 53 (1996) 16027–16034.
[15] M.M. Salleh, S. McDonald, H. Yasuda, A. Sugiyama, K. Nogita, Rapid Cu6Sn5 growth at liquid Sn/solid Cu interfaces, Scripta Mater. 100 (2015) 17–20.
[16] J. Li, P. Agyakwa, C. Johnson, Interfacial reaction in Cu/Sn/Cu system during the transient liquid phase soldering process, Acta Mater. 59 (2011) 1198–1211.
[17] C. Kao, Microstructures developed in solid-liquid reactions: using Cu-Sn reaction, Ni-Bi reaction, and Cu-In reaction as examples, Mater. Sci. Eng. A 238 (1997) 196–201.
[18] H.W. Tseng, C.Y. Liu, Evolution of Ag_3Sn compound formation in Ni/Sn5Ag/Cu solder joint, Mater. Lett. 62 (2008) 3887–3889.
[19] Y. Ye, Q. Wang, J. Lu, C. Liu, Y. Yang, High-entropy alloy: challenges and prospects, Mater. Today 19 (2016) 349–362.
[20] Q. He, Z. Ding, Y. Ye, Y. Yang, Design of high-entropy alloy: a perspective from nonideal mixing, JOM 69 (2017) 2092–2098.
[21] P.T. Vianco, A review of interface microstructures in electronic packaging applications: soldering technology, JOM 71 (2019) 158–177.
[22] K. Zeng, R. Stierman, T.C. Chiu, D. Edwards, K. Ano, K. Tu, Kirkendall void formation in eutectic SnPb solder joints on bare Cu and its effect on joint reliability, J. Appl. Phys. 97 (2005), 024508.
[23] H.Y. Hsiao, C.M. Liu, H.w. Lin, T.C. Liu, C.L. Lu, Y.S. Huang, C. Chen, K. Tu, Unidirectional growth of microbumps on (111)-oriented and nanotwinned copper, Sci 336 (2012) 1007–1010.
[24] D. Keller, U. Baither, G. Wilke, Schmitz, Mechanical properties of Pb-free SnAg solder joints, Acta Mater. 59 (2011) 2731–2741.
[25] O. Mokhtari, H. Nishikawa, Correlation between microstructure and mechanical properties of Sn–Bi–X solders, Mater. Sci. Eng. A 651 (2016) 831–839.
[26] J. Zhou, Y. Sun, F. Xue, Properties of low melting point Sn–Zn–Bi solders, J. Alloys Compd. 397 (2005) 260–264.